JACS
JOURNAL OF THE AMERICAN CHEMICAL SOCIETY

Article

pubs.acs.org/JACS

Stabilization of Scandium Terephthalate MOFs against Reversible Amorphization and Structural Phase Transition by Guest Uptake at Extreme Pressure

Alexander J. Graham,[†] Ana-Maria Banu,[‡] Tina Düren,[‡] Alex Greenaway,[§] Scott C. McKellar,[†] John P. S. Mowat,[§] Kenneth Ward,[†] Paul A. Wright,[§] and Stephen A. Moggach*,[†]

[†]EaStCHEM School of Chemistry and the Centre for Science at Extreme Conditions, The University of Edinburgh, King's Buildings, West Mains Road, Edinburgh EH9 3JJ, U.K.

[‡]Institute for Materials and Processes, School of Engineering, The University of Edinburgh, King's Buildings, Mayfield Road, Edinburgh, EH9 3JL, U.K.

[§]EaStCHEM School of Chemistry, University of St. Andrews, Purdie Building, St. Andrews, KY16 9ST, U.K.

Supporting Information

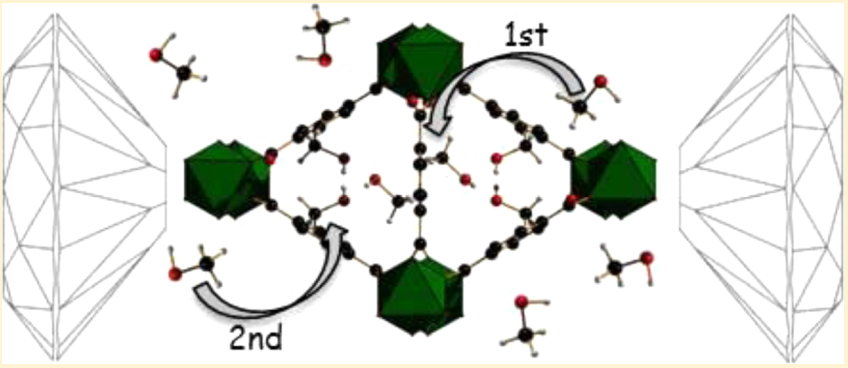

ABSTRACT: Previous high-pressure experiments have shown that pressure-transmitting fluids composed of small molecules can be forced inside the pores of metal organic framework materials, where they can cause phase transitions and amorphization and can even induce porosity in conventionally nonporous materials. Here we report a combined high-pressure diffraction and computational study of the structural response to methanol uptake at high pressure on a scandium terephthalate MOF (Sc_2BDC_3, BDC = 1,4-benzenedicarboxylate) and its nitro-functionalized derivative ($Sc_2(NO_2{-}BDC)_3$) and compare it to direct compression behavior in a nonpenetrative hydrostatic fluid, Fluorinert-77. In Fluorinert-77, Sc_2BDC_3 displays amorphization above 0.1 GPa, reversible upon pressure release, whereas $Sc_2(NO_2{-}BDC)_3$ undergoes a phase transition ($C2/c$ to $Fdd2$) to a denser but topologically identical polymorph. In the presence of methanol, the reversible amorphization of Sc_2BDC_3 and the displacive phase transition of the nitro-form are completely inhibited (at least up to 3 GPa). Upon uptake of methanol on Sc_2BDC_3, the methanol molecules are found by diffraction to occupy two sites, with preferential relative filling of one site compared to the other: grand canonical Monte Carlo simulations support these experimental observations, and molecular dynamics simulations reveal the likely orientations of the methanol molecules, which are controlled at least in part by H-bonding interactions between guests. As well as revealing the atomistic origin of the stabilization of these MOFs against nonpenetrative hydrostatic fluids at high pressure, this study demonstrates a novel high-pressure approach to study adsorption within a porous framework as a function of increasing guest content, and so to determine the most energetically favorable adsorption sites.

INTRODUCTION

Porous metal organic framework solids are of great current interest because of their potential applications and their chemical and structural variety, which lead directly to novel chemical and physical properties.[1] Their high surface areas, comprising internal pore surfaces that offer shape selectivity, variable hydrophobicity, accessible cations and organic functional groups, offer well-defined and readily tunable materials for molecular uptake, separation, storage and delivery, and in some cases catalytic conversion.[2,3] Furthermore, their complex structures are in many cases responsive to external stimuli such as temperature, light, and pressure.[4,5] Examination of the structural changes of microporous MOFs with increasing pressure is of fundamental interest,[6,7] because it reveals details of bonding within the framework and, where ingress of the pressure-transmitting fluid occurs, of framework−guest (and guest−guest) interactions. Further, efficient application of

Received: November 22, 2013
Published: May 19, 2014

dx.doi.org/10.1021/ja411934f | J. Am. Chem. Soc. 2014, 136, 8606−8613

MOFs at high pressure, for example in gas storage and separation, and as stationary phases in HPLC, will also require an understanding of the effect of high pressures on both framework and framework−guest structure.[8]

Diffraction studies, both X-ray and neutron, have yielded important information on both the response of frameworks to adsorption and the binding sites of guest molecules.[9−11] To date, there remains a relative paucity of structural data concerning adsorbate location in MOFs, so that even for molecules such as CO_2 that are of great current interest, only 66 entries within the Cambridge structural database exist (November 2012 release).[12] Even fewer studies have examined the response of single crystals of MOFs to high liquid pressures, because more specialized diamond anvil cell (DAC) apparatus is required, though recent computational and experimental studies have been performed at relatively low pressures, describing the framework collapse of MIL (*Matériaux de l'Institut Lavoisier*) materials.[13,14] Several high-pressure studies have now been reported on MOFs, including (but not exclusively) MOF-5 (zinc terephthalate), Cu-BTC (copper trimesate), and the zinc zeolitic imidazolate framework ZIF-8.[15−18] In these studies, the sample (single crystal or polycrystalline powder) was loaded into the DAC chamber and surrounded with a hydrostatic fluid by one of the following: Fluorinert FC-77 (a mixture of perfluorooctane (C_8F_{18}) and perfluorooxacyclononane ($C_8F_{16}O$)); diethylformamide; a 4:1 by volume mixture of methanol:ethanol; or a 16:3:1 methanol:ethanol:water mixture. Initial application of pressure to all three MOFs using a hydrostatic liquid comprising molecules small enough to enter the pores caused the frameworks to expand. Increasing pressure further resulted in more solvent molecules entering the pores, causing them to become "superfilled" with guest molecules, although with an associated decrease in the unit cell volume from its maximum value. However, because of the large size of the cages present in MOF-5, Cu-BTC, and ZIF-8, and the inherent disorder in the location of the adsorbate molecules, it was not possible to determine atomic positions of the adsorbed molecules in these cases.

The scandium terephthalate MOF, scandium 1,4-benzenedicarboxylate (Sc_2BDC_3) has a 3D framework structure, unique to this trivalent metal, with a high density of BDC groups linking isolated ScO_6 octahedra.[19] Projected down the *a*-axis in the orthorhombic (room temperature) form of Sc_2BDC_3, the triangular channels (~4 Å in free diameter) appear one-dimensional (Figure 1a), but there are small gaps in the "walls" of these channels between adjacent BDC ligands. Two symmetry-independent BDC molecules exist; the first is bisected by two perpendicular 2-fold axes and penetrated by a third (Group 1, Figure 1b), while the other has an inversion center at the center of the BDC ring (Group 2, Figure 1c). The windows formed between pairs of Group 1 and Group 2 linkers form interconnecting channels along the *c*- and *b*-axes directions respectively, giving rise to a three-dimensionally porous framework structure. The pores are hydrophobic; after synthesis they contain no solvent or water molecules. The relatively high porosity of Sc_2BDC_3 and its thermal and chemical stability, together with its tendency to form high-quality single crystals, make it a model MOF system for studies of small-molecule adsorption. In situ diffraction studies of Sc_2BDC_3 at low temperatures (~230 K) and moderate gas pressures (1−5 bar) have located small gas molecules such as CO_2 and light hydrocarbons physisorbed in the pores, and

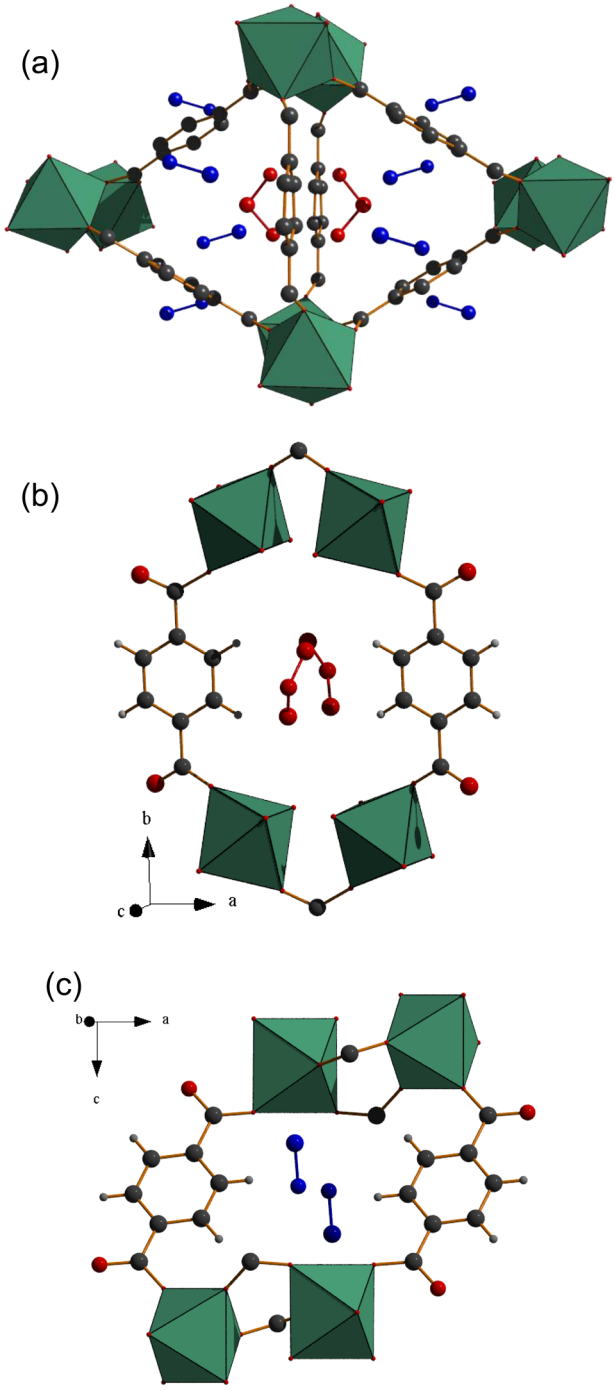

Figure 1. (a) Triangular pores formed in Sc_2BDC_3 viewed along the *a*-axis. Disordered methanol molecules are represented by solid red (Site 1) and blue (Site 2) colored molecules. Openings between triangular channels of Sc_2BDC_3 between (b) Group 1 and (c) Group 2 ligands as viewed along the *c* and *b*-axes, respectively. Key: C, gray; ScO_6 octahedra, green; O, red; H, light gray.

determined that upon CO_2 uptake the structure relaxed to better coordinate the adsorbate molecules, with a resultant displacive phase transition and associated symmetry change (*Fddd* to *C*2/*c*).[20] The spatial constraints imposed by the narrow pores on the configuration and packing of adsorbate molecules are partly responsible for their ordering and subsequent accurate location by diffraction. A similar approach, in which compounds have been adsorbed into MOFs and their

dx.doi.org/10.1021/ja411934f | J. Am. Chem. Soc. 2014, 136, 8606−8613

structure determined as part of the resultant guest−host complex has recently been exploited to determine the molecular structure of compounds available only on the nanogram scale or which cannot readily be crystallized.[21]

Here we report structural studies of Sc_2BDC_3 at high pressures (0.1−2.3 GPa) in the presence of different hydrostatic liquids that are either nonpenetrative (fluorinated hydrocarbon) or adsorbing (methanol). Whereas the empty structure shows reversible amorphization at elevated pressures, the methanol-containing structure is greatly stabilized and is the first "high pressure" example where the adsorbates are located crystallographically and the host−guest and guest−guest interactions explored and elucidated by complementary computer simulation.

It is also possible to prepare single crystals of the nitro-functionalized analogue of this structure, $Sc_2(NO_2{-}BDC)_3$ by direct synthesis. The presence of the bulky nitro groups causes the framework to distort to monoclinic $C2/c$ symmetry to accommodate them, with associated reduction in the free space. The nitro groups block the channels to N_2 uptake at 77 K, but permit some uptake of CO_2 at 273 K.[19] Our high-pressure studies of this nitro-functionalized scandium MOF show very different behavior to that of the unfunctionalized form, for it undergoes a high-pressure phase transition that results in a strong volume decrease when empty, but this is inhibited by methanol uptake over the pressure range explored.

Taken together, these high-pressure structural studies of the parent and the functionalized Sc_2BDC_3 MOF represent the first ever reported inclusion of ordered guest molecules into the pores of a MOF as a function of high pressure and reveal both the atomistic ordering of adsorbates in the pores and the resulting stabilization of frameworks against major structural changes.

EXPERIMENTAL SECTION

Single crystals of Sc_2BDC_3 and its nitro-derivative were prepared via solvothermal and hydrothermal routes, respectively.[19,22] Crystals of Sc_2BDC_3 and $Sc_2(NO_2{-}BDC)_3$ were loaded individually into a modified Merrill-Bassett diamond anvil cell (DAC) along with a ruby crystal (to act as a pressure calibrant). Both crystals were surrounded with a liquid in order to ensure pressure was applied hydrostatically to the crystals. In the first experiments on each crystal type, high-pressure experiments were performed using a nonpenetrating hydrostatic medium, the fluorinated hydrocarbon Fluorinert FC-77, whereas a second set of experiments was performed using methanol as the pressure medium, which was found to enter the pore system of these MOFs. For comparison, the structure of Sc_2BDC_3 was also measured at room temperature when immersed in liquid methanol without externally applied pressure. In addition, the adsorption (and desorption) isotherms of methanol from the vapor phase was measured on a Hiden IGA2 gravimetric analyzer for Sc_2BDC_3 and $Sc_2(NO_2{-}BDC)_3$ at 303 and 298 K up to the saturation pressures at these temperatures.

Complementary grand canonical Monte Carlo (GCMC)[23] simulations were performed in order to study the order in which adsorption sites are filled by methanol molecules in Sc_2BDC_3, while molecular dynamics[17] simulations were performed in order to elucidate the pore-filling mechanism. The use of GCMC and molecular dynamics simulations to understand site ordering of guest molecules has been used in recent years for understanding gas sorption into MOFs,[24−26] though to our knowledge, this is the first time they have been applied to pressurized structures. For more details see the Supporting Information (SI).

RESULTS AND DISCUSSION

Compression of Sc_2BDC_3 Using Fluorinert FC-77. On loading a crystal of Sc_2BDC_3 in Fluorinert FC-77 to 0.1 GPa, the unit cell volume decreases by 39 Å^3 (0.6%) compared to the ambient pressure "empty" structure. On increasing the pressure further to 0.4 GPa, a crystalline-to-amorphous phase transition took place which was accompanied by an optical change in the crystal from colorless to opaque (Figure 2a). This transition is well below the hydrostatic limit of the medium (0.95 GPa), and is therefore not caused by nonhydrostatic conditions.[27] The Raman spectra collected within the fingerprint region of the spectra (100 to 1300 cm^{-1}) were almost identical (Figure S1 in the SI), which suggests that the local structure of Sc_2BDC_3 in the amorphous phase is retained. The pressure was released to ambient pressure, and the crystal returned from opaque to colorless (Figure 2b). Single-crystal X-ray diffraction data collected on the recovered crystal confirmed that the amorphization was fully reversible, with the structure reverting back to the original crystalline phase. The fact that the transition is reversible further supports the assumption that the framework remains intact during the transition. The phenomenon of pressure-induced amorphization has been known for several years, with amorphous ice being the most well-known example.[28] Reversible pressure-induced amorphization has been observed previously in zeolites which have the LTA structure type[29] and inorganic materials such as $CsAuI_3$[30] and $Ge_2Sb_2Te_5$.[31] More recently, the reversible pressure-induced amorphization of the dense zeolitic imidazole framework ZIF-4 ([Zn(Im)2], Im = imidazolate) was observed between 0.35 and 0.98 GPa for the evacuated sample, or 1.49−4.54 GPa for the solvent-containing sample.[32] The compressibility behavior observed here in Sc_2BDC_3 is therefore very similar to that observed in ZIF-4, with a crystalline−amorphous phase transition observed upon direct compression of the bare framework at low pressures (~<1 GPa; similar to the evacuated sample of ZIF-4). Not all MOFs exhibit reversible crystalline−amorphous transitions. In ZIF-8 and MOF-5, amorphization is irreversible, though it can play a vital role in the capture and storage of gases that are harmful to the environment.[33,34] The smaller pore nature (and higher density) of Sc_2BDC_3 would therefore appear to afford it some resilience to irreversible amorphization at lower pressures on directly compressing the

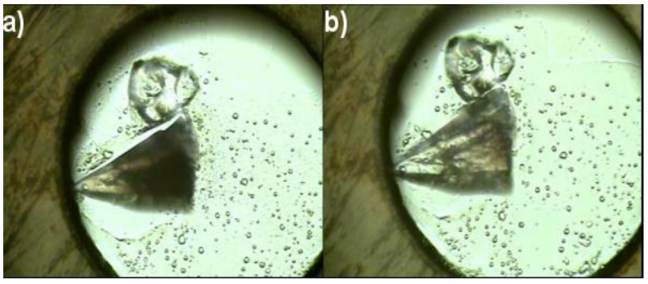

Figure 2. Optical image of Sc_2BDC_3 (lower crystal) loaded in Fluorinert FC-77 at (a) 0.40 GPa and (b) 0.10 GPa after decompression. The colorless crystal sitting above Sc_2BDC_3 is a chip of ruby, which is used as a pressure calibrant. The gasket hole is 300 μm in diameter.

dx.doi.org/10.1021/ja411934f | J. Am. Chem. Soc. 2014, 136, 8606−8613

crystalline phase. This is an area worth investigating further as irreversible transitions tend to have a detrimental effect on the adsorption capabilities of MOFs.

Compression of Sc_2BDC_3 Using Methanol. Upon immersion of a crystal of Sc_2BDC_3 in methanol without added pressure (in a capillary), the unit cell expanded as methanol diffused into the framework (Table 1, Figure 1a). The

Table 1. Number of Methanol Molecules, Methanol Density, Occupancy of Site 1 and Site 2 Methanol Molecules (calculated using the SQUEEZE algorithm) in Sc_2BDC_3 Are Shown[a]

pressure (GPa)	total no. of MeOH molecules/unit cell	MeOH density (g cm^{-1})	occupancy of Site-1 MeOH molecules	occupancy of Site-2 MeOH molecules
0.0	9	0.23	0.5	0.39
0.3	32	0.76	1.0	0.49
0.6	39	0.91	1.0	0.71
1.1	41	0.96	1.0	0.79
1.4	38	0.92	1.0	0.69
1.6	42	1.01	1.0	0.80
2.3	39	0.98	1.0	0.75

[a]Freely refined occupancies from the model are given in Table S1 in the SI. The 0.0 GPa data set refers to Sc_2BDC_3 which was "immersed" in methanol at ambient pressure at 298 K.

density of methanol modeled in the pores equates to an uptake of 3.3 mmol g^{-1}, in reasonable agreement with the experimental isotherm which shows a reversible uptake of ~4 mmol g^{-1} (or 1.2 molecules per triangular "channel", Figure S2 in the SI).

A separate single crystal was then loaded into a DAC using methanol as the hydrostatic liquid. On loading to 0.3 GPa, the unit cell volume expanded further, as a result of additional methanol being forced into the porous framework (Table 1). Although the inclusion of small molecules has been observed before in the pores of much larger MOFs (with nanosized cavities) at high pressure, these were not ordered in the pores.[15−17] Expansion of the framework continued to 0.6 GPa, with the unit cell volume increasing by 41.4 $Å^3$ (0.7%). On increasing the pressure to 1.1 GPa, the volume began to decrease, and the cell volume continuously decreased up to 3.0 GPa (Figure 3a). The compressibility of the unit cell dimensions is strongly anisotropic (Figures S3−S5 in the SI) so that while the *a*-axis follows the same trend as the unit cell volume, showing an initial increase up to 1.1 GPa, followed by a continuous decrease to 3.0 GPa, both the *b* and *c*-axes decrease in length for the entirety of the increasing pressure regime.

The anisotropic compression of the unit cell dimensions (and volume) can be explained by analyzing the uptake of methanol molecules within the pores of Sc_2BDC_3. Inclusion of methanol molecules does not result in a change of symmetry, unlike the transition from *Fddd* to *C*2/*c* on uptake of CO_2 guest molecules observed previously. On initially surrounding the sample with methanol at ambient pressure, the guest molecules occupy two distinct sites, though the identity of the non-hydrogen atoms could not be identified. Site 1 (Figure 1a,b) is only half occupied at ambient pressure (and disordered about a 2-fold axis). Pairs of Site 1 methanol molecules sit on either side of the "gaps" formed between Group 1 ligands. Site 2 is also only partially occupied at ambient pressure and is located on either side of the "gaps" between Group 2 ligands (Figure 1a,c). Site 1 and Site 2 molecules occupy the channels which

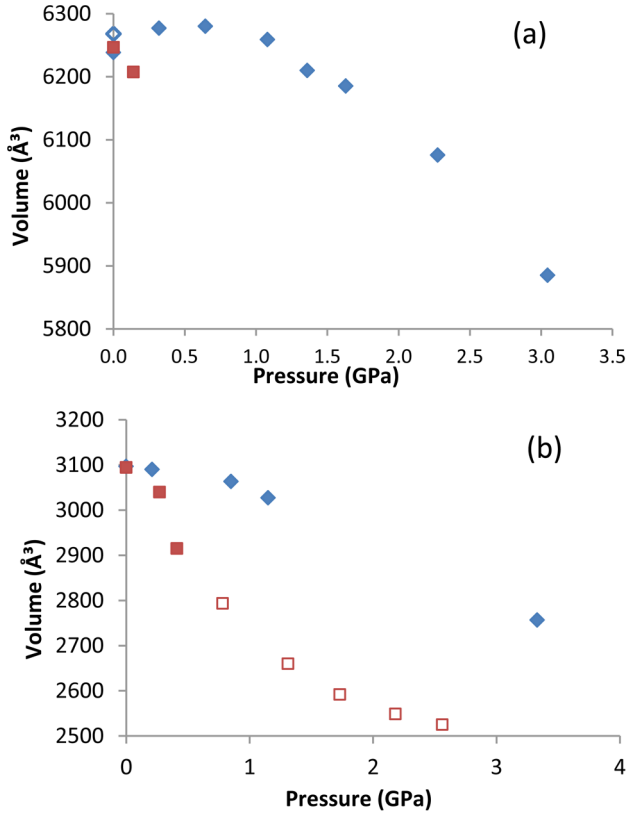

Figure 3. Unit cell volume of (a) Sc_2BDC_3 and (b) $Sc_2(NO_2–BDC)_3$ in methanol (blue diamonds) and Fluorinert FC-77 (red squares) as a function of pressure. In (a) the open blue diamond refers to the ambient structure surrounded with MeOH in a capillary. In (b) the closed and open red squares refer to the *C*2/*c* and *Fdd*2 structures respectively, with the unit cell halved for the latter. Error bars are smaller than the symbols.

run along the *a*-axis, resulting in a stacking of methanol molecules along the principal pore direction (Figure 1). The *a*-axis expands on uptake of methanol, so it appears that the filling of both sites and subsequent stacking of methanol molecules along the pore direction is responsible for the expansion of the *a*-axis and contraction along the *b*- and *c*-axes. Such behavior is often observed during negative linear expansion, for example in "wine-rack" (or similar) framework topologies.[35]

On increasing pressure to 0.3 GPa, Site 1 becomes fully occupied, while the Site 2 occupancy also increases (to 0.5). On increasing pressure above 0.3 GPa, the occupancy of Site 2 molecules continues to increase, reaching a peak occupancy of 0.8 at 1.1 GPa. Increase of the *a*-axis (and volume expansion) continues to 0.6 GPa as more methanol molecules occupy Site 2. The non-hydrogen atom bonding distances between pairs of Site 1 (2.701 Å) and Site 2 (2.422 Å) molecules at 0.6 GPa is in the range of H-bonding interaction distances observed for hydroxyl groups in the solid state, although the guest−guest distance between pairs of Site 2 molecules is toward the lower end of this range. The minimum O···O distance in methanol crystallized at 4.0 GPa (~40,000 bar), for example, measures 2.425 Å.[36] We postulate that the increased uptake at higher pressures, resulting in short guest−guest contact distances is the reason why Site 2 is not readily fully occupied.

Contraction of both the *a*-axis and volume starts to occur above 0.6 GPa, where the swelling effect caused by continuous inclusion of methanol molecules stacking along the *a*-axis is

dx.doi.org/10.1021/ja411934f | J. Am. Chem. Soc. 2014, 136, 8606−8613

overcome. Instead, compression of the *a*-axis, and therefore volume reduction, is favored. A similar effect was observed in Cu-BTC, which initially expands on increasing pressure to 0.5 GPa, then compresses on increasing pressure further to 1.3 GPa even though more solvent fills the pores.[17] No appreciable increase in methanol density is observed above 1.1 GPa, and therefore direct compression of the framework takes place to 3.0 GPa. Amorphization of Sc_2BDC_3 in methanol does not take place up to 3.0 GPa. This behavior is not dissimilar to that of MOF-5, where the onset of amorphization can be delayed by guest inclusion, with MOF-5 becoming amorphous above 3.2 GPa upon hydrostatic compression using diethylformamide as a hydrostatic medium.[16] More recently, in a high-pressure study of the flexible framework NH_2-MIL-53-(In), guest inclusion also occurs, and pressure-induced amorphization does not take place until >20 GPa.[37]

GCMC simulations were performed in order to understand site filling by methanol molecules in Sc_2BDC_3 and to determine whether the orientations (C and O positions) of the methanol molecules can be determined. Density distributions of adsorption sites were obtained as a function of loading for the structures obtained at ambient pressure, and 0.6 GPa, in order to elucidate whether any subtle changes in the framework at higher pressures gave rise to preferential adsorption sites, as seen previously for CO_2 in Sc_2BDC_3. No differences were observed (see Figure S6 in the SI), so that only the simulations on the structure determined at 0.6 GPa are shown here. At low loading in both the ambient and 0.6 GPa structures, methanol molecules are preferentially adsorbed at Site 1 (Figure 4). As loading increases to 21 molecules/unit cell (mol./uc.), Site 1 becomes saturated, and adsorption of methanol molecules at Site 2 begins in both the ambient and 0.6 GPa structures. A further increase in loading (beyond 32 mol./uc.) results in a greater uptake of methanol molecules at Site 2. The pore filling order of both sites would therefore appear to match the order of uptake of methanol molecules observed in our high-pressure experiments and is independent of any subtle changes in the framework at elevated pressures.

In an effort to further elucidate the pore-filling mechanism and examine further guest−guest interactions, molecular dynamics simulations were performed using the framework Sc_2BDC_3 structure measured when immersed in methanol, as well as for each of the structures in Table 1, at a loading of 39−41 mol./u.c. This corresponds to a fully saturated framework, with three methanol molecules per pore.

In order to determine whether the adsorbed molecules interact with each other through hydrogen bonds, radial distribution functions were calculated from the molecular dynamics simulations by analyzing the distances between the oxygen and hydroxyl H atoms of different molecules of adsorbed methanol, and H-bonds were located in the MD snapshots. Such an analysis should determine the origin of the preferred uptake in Site 1, as well as suggesting the most likely orientation of methanol molecules in the sites, because it was not possible to distinguish CH_3 and OH groups by XRD. Therefore, we determined site-specific radial distribution functions distinguishing between atoms in pairs of methanol molecules with the following locations: Site 1−Site 1; Site 2−Site 2, Site 1−Site 2). Only distances between atoms of different molecules were examined. Similar results were observed for all high-pressure data sets−only the results obtained by modeling using the framework positions determined in contact with 0.6 GPa of methanol are shown here (Figure 5).

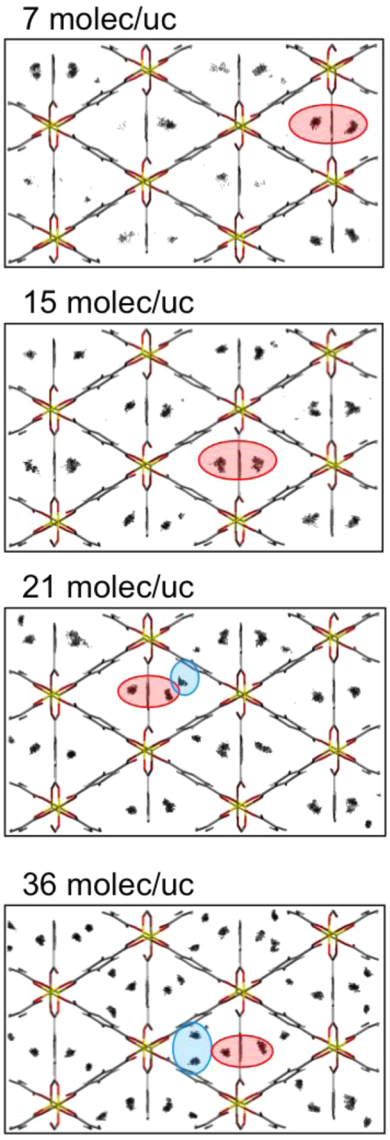

Figure 4. Density distribution plots for the adsorption of methanol in Sc_2BDC_3. Each plot shows the locations of methanol molecules adsorbed at a particular loading. Each dot represents the position of the center of mass of a molecule during the GCMC simulation. Red and blue regions denote adsorption at Site 1 and Site 2, respectively.

For three of the four atomic pairs analyzed, the separation distance between oxygen and hydrogen atoms lies between 1.50 and 2.25 Å, characteristic for hydrogen bonds (Figure 5). The highest occurrence of hydrogen bonds occurs between pairs of Site 1 methanol molecules. Methanol molecules adsorbed on Site 2 are equally likely to form hydrogen bonds with other Site 2 molecules and also with hydrogen atoms of methanol molecules adsorbed within the same pore at Site 1. By contrast, oxygen atoms of methanol molecules adsorbed on Site 1 only rarely form hydrogen bonds with hydrogen atoms of methanol molecules at Site 2. The presence of hydrogen bonds of type Site 1-to-Site 1, Site 2-to-Site 2, and Site 2-to-Site 1 is illustrated in the simulation snapshot of the "immersed" ambient pressure structure (Figure 6). Site 1 methanol molecules exhibit a strong preference for hydrogen bonding to other Site 1 molecules, indicating that the arrangement of framework atoms near Site 1

dx.doi.org/10.1021/ja411934f | J. Am. Chem. Soc. 2014, 136, 8606−8613

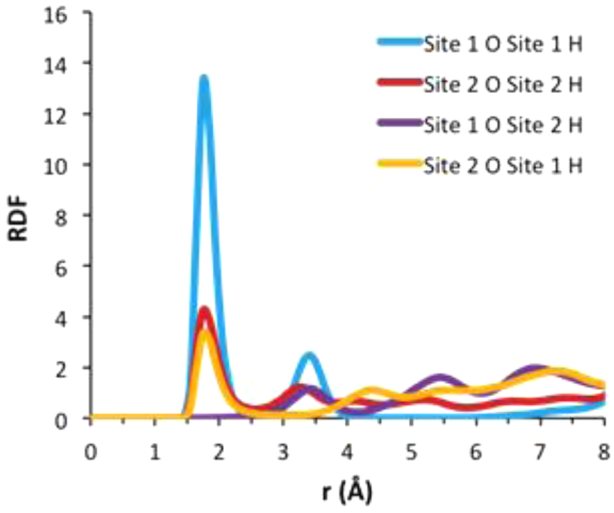

Figure 5. Radial distribution functions for methanol molecules adsorbed in Sc_2BDC_3. Site 1 O corresponds to the O atom of a methanol molecule adsorbed on Site 1, Site 2 H to the OH group H atom of a methanol molecule adsorbed on Site 2, and so on.

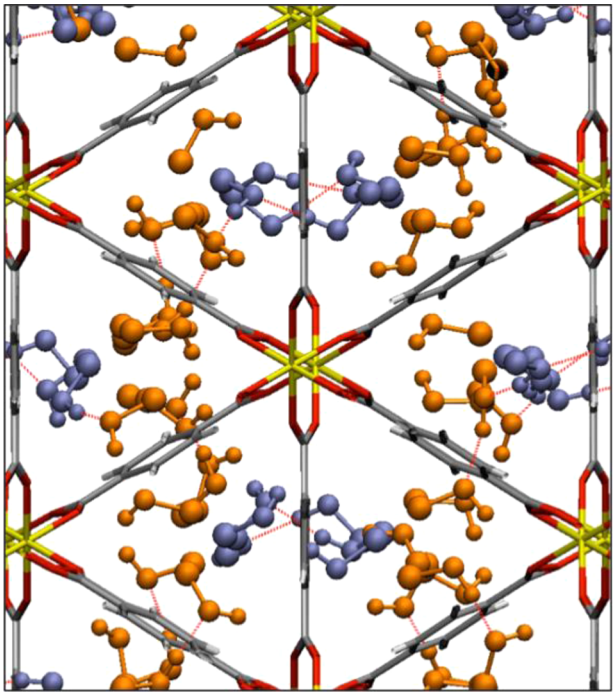

Figure 6. Arrangement of methanol molecules within Sc_2BDC_3 from the immersed ambient pressure structure coordinates. Molecules adsorbed at Site 1 are shown in blue, while molecules adsorbed at Site 2 are shown in orange. Hydrogen bonds are indicated using red dashed lines.

is more conducive to hydrogen-bond formation than the geometry at Site 2. The snapshot also suggests that orientation of methanol C and O atoms with the O atoms closer to the gaps (and other Site 1 methanol molecules) is favored. The high incidence of hydrogen bonds between pairs of Site 1 molecules increases the site stability and results in a preferential filling of Site 1. By contrast, methanol molecules adsorbed at Site 2 are able to form hydrogen bonds less frequently and exhibit no preference in interacting with Site 1 or Site 2 methanol molecules.

Compression of $Sc_2(NO_2–BDC)_3$ using Fluorinert FC-77. In order to determine the effect of derivatizing the terephthalate linker on the uptake of guest molecules at pressure, the effect of pressure on $Sc_2(NO_2–BDC)_3$ was also studied. At ambient pressure and temperature, $Sc_2(NO_2–BDC)_3$ adopts monoclinic $C2/c$ symmetry; a = 8.6786(3) Å, b = 34.4286(13) Å, c = 11.0628(4) Å, β = 110.482(2)° and V = 3096.4(2) Å^3. Topologically, the framework is very similar to the native Sc_2BDC_3 structure composed of the same 1D channels (Figure 7). However, the bulky NO_2 group is partially

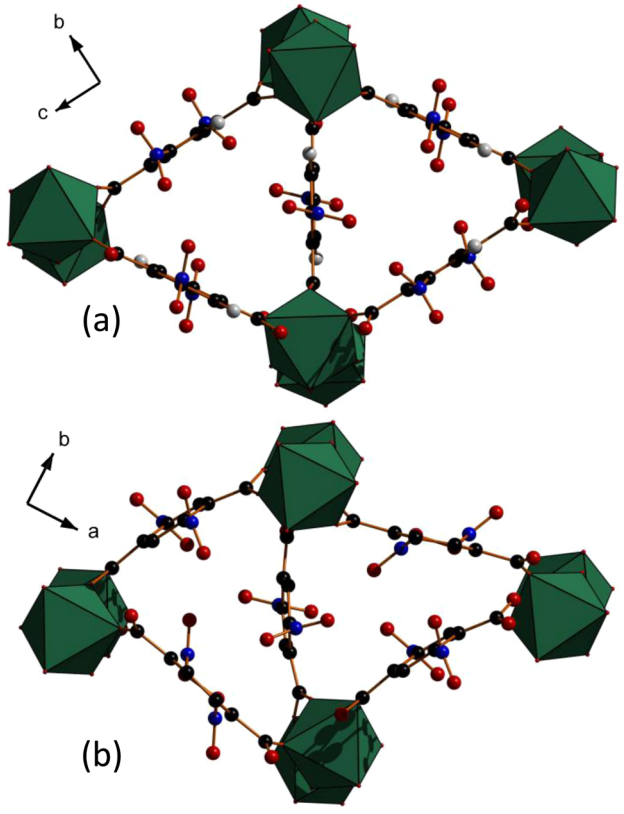

Figure 7. Structural phase transition of (a) $Sc_2(NO_2–BDC)_3$ to (b) $Sc_2(NO_2–BDC)_3$-HP at 0.8 GPa. Note: the ScO_6 octahedra tilt, causing the collapse of the porous network. Color scheme: O, red; C, gray; N, blue and ScO_6 octahedra, green.

ordered on each of the two ligands (retaining statistical disorder over two positions by an inversion center in Group 1 and by a 2-fold rotation axis in Group 2). This results in distortion of the structure and lowering of the symmetry from *Fddd* to *C*2/*c*. The resultant structure has no aperture between pairs of Group 1 or Group 2 ligands (assuming no ligand rotation) and a reduced pore volume.

In order to ascertain whether a crystalline-to-amorphous phase transition is observed in $Sc_2(NO_2–BDC)_3$ at high pressure (as was observed with Sc_2BDC_3), and to deconvolute the effect of pressure and solvent inclusion, a separate high-pressure experiment was carried out on $Sc_2(NO_2–BDC)_3$ using Fluorinert FC-77. On increasing pressure from ambient to 0.3 GPa, direct compression of the framework occurs, and is reflected in the compressibility of all three axes and the volume (Figure 3b, and Figures S8–S10 in the SI). On increasing pressure further to 0.8 GPa, a single-crystal to single-crystal phase transition occurs with a resulting crystallographic symmetry change from space group *C*2/*c* to *Fdd*2; a =

dx.doi.org/10.1021/ja411934f | J. Am. Chem. Soc. 2014, 136, 8606–8613

19.610(6) Å, b = 32.864(8) Å, c = 8.6757(16) Å, and V = 5591(2) Å^3. The new phase ($Sc_2(NO_2{-}BDC)_3$-HP), is formed by a rotation of the ScO_6 octahedra and is characterized by a drastic distortion (and collapse) of the 1-D porous channels (Figure 7). Above 0.8 GPa, the framework volume continued to reduce with the compressibility decreasing with increasing pressure. Above 2.6 GPa, the sample underwent an irreversible amorphization. This amorphization pressure for the nitro-form is much higher than that for Sc_2BDC_3 (0.4 GPa), indicating the stabilization effect of the presence of the bulk nitro group. The compressibility of the $Sc_2(NO_2{-}BDC)_3$-HP phase is anisotropic, with the ∼8 Å axis (previously the a-axis in $Sc_2(NO_2{-}BDC)_3$) actually increasing (modestly by 0.03 Å) in length between 0.8 to 2.2 GPa. Unlike the guest-driven increase in the ∼8 Å a-axis observed for the native Sc_2BDC_3, the increase here is actually caused by a continued tilting of the ScO_6 octahedra to higher pressures. The gradient of the unit cell compression decreases in Fluorinert FC-77 as a function of pressure as the sample becomes less compressible with increasing pressure (Figure 3b). This behavior is typical for molecular materials where direct compression takes place.

Compression of $Sc_2(NO_2{-}BDC)_3$ using Methanol. On initially loading a crystal of $Sc_2(NO_2{-}BDC)_3$ to 0.21 GPa using methanol as the hydrostatic medium, the unit cell volume decreased by 32.69 Å^3 (0.52%, Figure 3b). Increasing pressure further to 0.9 GPa, the volume continued to decrease; above 0.9 GPa, a volume decrease is observed which continued to 3.3 GPa. Unfortunately, unlike the unfunctionalized Sc_2BDC_3 sample, the high-pressure data was not of high enough quality to be able to extract atomic structural information on the pore contents, or to model the uptake of solvent. Nevertheless, the contrasting compression behavior when compared with a nonpenetrative hydrostatic fluid (Figure 3b) indicates that methanol uptake does occur, and that its inclusion stabilizes the framework against structural transition and very rapid volume decrease (as observed in Fluorinert). On increasing pressure to 0.2 GPa, and then further to 0.9 GPa, the a-axis increases (by 0.11%), while the b- and c-axes both decrease by 0.13 and 0.28% respectively (Figure S11 to S13 in the SI). This behavior is similar in type to that of Sc_2BDC_3 in methanol, where the axis along which the porous channels of the framework run (which is also the ∼8 Å a-axis), increases in length. The increase in length of the a-axis in $Sc_2(NO_2{-}BDC)_3$, is much less drastic, and this reflects the lower uptake. This is unsurprising, considering the presence of the bulky NO_2 side groups, with the overall effect of pressure causing a volume reduction to 0.9 GPa, rather than expansion which is observed in Sc_2BDC_3 to 0.6 GPa. This result is also consistent with the methanol adsorption isotherm under ambient pressure conditions, which shows a significantly reduced uptake of methanol compared to the native Sc_2BDC_3 (Figure S2 in the SI).

Above 0.9 GPa, the a-axis (and volume) contracts more rapidly. This behavior is typical of porous MOFs which display two regions of different compressibility. In Cu-BTC, this transitional behavior was attributed to an initial hyperfilling of the pores by the hydrostatic liquid followed by a sustained compression of the filled pores at higher pressures, resulting in a material which becomes more compressible at higher pressures.[15,17] In our single-crystal study of Cu-BTC, this transition was attributed to a sudden emptying of the pores at higher pressures.[17] The differences observed between single-crystal and powder data in Cu-BTC is related to the different approaches used and sample size. In the study by Chapman et al., for example, pressure dependence on uptake of hydrostatic media was also shown to be crystallite size dependent. We, however, cannot conclude that this occurs in $Sc_2(NO_2{-}BDC)_3$, as similar behavior is observed in Sc_2BDC_3, where the methanol content actually reached saturation by 1.1 GPa, and remains in the pores until at least 2.3 GPa.

■ CONCLUSIONS

The compressibility of both Sc_2BDC_3 and $Sc_2(NO_2{-}BDC)_3$ MOFs are highly sensitive to the pressure-transmitting medium used. For Sc_2BDC_3 in Fluorinert FC-77, the molecules are too bulky to penetrate the pore volume, and so the framework compresses upon loading to 0.1 GPa. Increasing the pressure further to 0.4 GPa results in a crystalline-to-amorphous phase transition which is fully reversible. Raman spectroscopy suggests that loss of crystallinity is possible without bond breaking. Using methanol as a medium, molecules enter the pores of Sc_2BDC_3 and can be located in two distinct sites, Sites 1 and 2. The first is filled by 0.3 GPa: upon increasing pressure, the occupancy of the less favorable Site 2 increases as more methanol molecules are forced into the pores until a maximum uptake is observed at ∼1.1 GPa. The crystallinity of Sc_2BDC_3 is retained during methanol-mediated compression up to 3.0 GPa, well beyond the limit where no further methanol uptake occurs. This behavior was further investigated using both GCMC and molecular dynamics simulations, which further supported the order of inclusion of adsorbed methanol molecules, filling Site 2 at higher pressures. The propensity for hydrogen bonding was also investigated and indicates that H-bonding interactions occur between molecules in each site and that H-bonding between adjacent Site 1 molecules helps orient the methanol molecules.

The pore volumes in $Sc_2(NO_2{-}BDC)_3$ are smaller than those in Sc_2BDC_3 due to the nitro groups. This alters the way in which the unit cell volume changes in order to accommodate increasing pressure. As is the case with Sc_2BDC_3, compressing $Sc_2(NO_2{-}BDC)_3$ to 0.4 GPa in Fluorinert FC-77 resulted in direct compression of the framework, but increasing the pressure further to 0.8 GPa resulted in a single-crystal to single-crystal phase transition ($C2/c$ to $Fdd2$) with a concomitant distortion of the 1-D porous channels. Between 0.8 and 2.6 GPa, the framework showed continued reduction in volume with the compressibility decreasing with increasing pressure. Above 2.6 GPa, the sample underwent an irreversible amorphization, though the pressure at which this happens is 6.5 times greater than that for the unfunctionalized Sc_2BDC_3, demonstrating the increased stability of the crystalline phase of the framework containing the derivatized BDC ligand. In Sc_2BDC_3, the pressure-induced inclusion of methanol caused a swelling of the unit cell, whereas in $Sc_2(NO_2{-}BDC)_3$ we only see a decrease in volume; it is likely that the uptake of methanol is much lower. The high-pressure data for $Sc_2(NO_2{-}BDC)_3$ is not of high enough quality to extract pore content information, but methanol uptake in $Sc_2(NO_2{-}BDC)_3$ is observed at ambient pressures and can be inferred to take place at high pressures from the increase in stability of the $C2/c$ phase and its compressibility behavior.

The use of high pressures to saturate the pores of MOFs with guest molecules has several possible future applications, the most obvious of which is in the use of pressure to post-modify MOFs by flooding the pores with reactive species, overriding the use of diffusion techniques. The use of gaseous pressure

dx.doi.org/10.1021/ja411934f | J. Am. Chem. Soc. 2014, 136, 8606−8613

media could also be used for future CO_2 and N_2 activation within MOFs, as diffusion of high-concentrations of gases would be possible at elevated pressures.

■ ASSOCIATED CONTENT

Supporting Information

Crystallographic information files (CIFs), experimental methods, and supplementary compression data. This material is available free of charge via the Internet at http://pubs.acs.org.

■ AUTHOR INFORMATION

Corresponding Author

s.moggach@ed.ac.uk

Notes

The authors declare no competing financial interest.

■ ACKNOWLEDGMENTS

We thank the Royal Society of Edinburgh and the Scottish Government for a fellowship to Dr. Stephen A. Moggach and the EPSRC for a Postdoctoral Prize for Dr. John Mowat. We also thank the EPSRC (EP/J02077X/; EP/F009208/1), and The Leverhulme Trust for financial support through a research project grant.

■ REFERENCES

(1) Zhou, H.-C.; Long, J. R.; Yaghi, O. M. *Chem. Rev.* **2012**, *112*, 673.
(2) Čejka, J. *Angew. Chem., Int. Ed.* **2012**, *51*, 4782.
(3) Mitchell, L.; Gonzalez-Santiago, B.; Mowat, J. P. S.; Gunn, M. E.; Williamson, P.; Acerbi, N.; Clarke, M. L.; Wright, P. A. *Catal. Sci. Technol.* **2013**, *3*, 606.
(4) Feng, P. L.; Leong, K.; Allendorf, M. D. *Dalton Trans.* **2012**, *41*, 8869.
(5) Modrow, A.; Zargarani, D.; Herges, R.; Stock, N. *Dalton Trans.* **2011**, *40*, 4217.
(6) Gagnon, K. J.; Beavers, C. M.; Clearfield, A. *J. Am. Chem. Soc.* **2013**, *135*, 1252.
(7) Ma, Q.; Yang, Q.; Ghoufi, A.; Ferey, G.; Zhong, C.; Maurin, G. *Dalton Trans.* **2012**, *41*, 3915.
(8) Zhang, M.; Pu, Z.-J.; Chen, X.-L.; Gong, X.-L.; Zhu, A.-X.; Yuan, L.-M. *Chem. Commun.* **2013**, *49*, 5201.
(9) Couck, S.; Gobechiya, E.; Kirschhock, C. E. A.; Serra-Crespo, P.; Juan-Alcañiz, J.; Martinez Joaristi, A.; Stavitski, E.; Gascon, J.; Kapteijn, F.; Baron, G. V.; Denayer, J. F. M. *ChemSusChem* **2012**, *5*, 740.
(10) Wu, H.; Simmons, J. M.; Srinivas, G.; Zhou, W.; Yildirim, T. *J. Phys. Chem. Lett.* **2010**, *1*, 1946.
(11) Xiang, S.; He, Y.; Zhang, Z.; Wu, H.; Zhou, W.; Krishna, R.; Chen, B. *Nat. Commun.* **2012**, *3*, 954.
(12) Allen, F. H.; Motherwell, W. D. S. *Acta Crystallogr., Sect. B* **2002**, *58*, 407.
(13) Yot, P. G.; Ma, Q.; Haines, J.; Yang, Q.; Ghoufi, A.; Devic, T.; Serre, C.; Dmitriev, V.; Ferey, G.; Zhong, C.; Maurin, G. *Chem. Sci.* **2012**, *3*, 1100.
(14) De Malsche, W.; Van der Perre, S.; Silverans, S.; Maes, M.; De Vos, D. E.; Lynen, F.; Denayer, J. F. M. *Microporous. Mesoporous Mater.* **2012**, *162*, 1.
(15) Chapman, K. W.; Halder, G. J.; Chupas, P. J. *J. Am. Chem. Soc.* **2008**, *130*, 10524.
(16) Graham, A. J.; Allan, D. R.; Muszkiewicz, A.; Morrison, C. A.; Moggach, S. A. *Angew. Chem., Int. Ed.* **2011**, *50*, 11138.
(17) Graham, A. J.; Tan, J.-C.; Allan, D. R.; Moggach, S. A. *Chem. Commun.* **2012**, *48*, 1535.
(18) Moggach, S. A.; Bennett, T. D.; Cheetham, A. K. *Angew. Chem., Int. Ed.* **2009**, *48*, 7087.
(19) Mowat, J. P. S.; Miller, S. R.; Griffin, J. M.; Seymour, V. R.; Ashbrook, S. E.; Thompson, S. P.; Fairen-Jimenez, D.; Banu, A.-M.; Düren, T.; Wright, P. A. *Inorg. Chem.* **2011**, *50*, 10844.
(20) Miller, S. R.; Wright, P. A.; Devic, T.; Serre, C.; Férey, G. r.; Llewellyn, P. L.; Denoyel, R.; Gaberova, L.; Filinchuk, Y. *Langmuir* **2009**, *25*, 3618.
(21) Inokuma, Y.; Yoshioka, S.; Ariyoshi, J.; Arai, T.; Hitora, Y.; Takada, K.; Matsunaga, S.; Rissanen, K.; Fujita, M. *Nature* **2013**, *495*, 461.
(22) Mowat, J. P. S.; Seymour, V. R.; Griffin, J. M.; Thompson, S. P.; Slawin, A. M. Z.; Fairen-Jimenez, D.; Duren, T.; Ashbrook, S. E.; Wright, P. A. *Dalton Trans.* **2012**, *41*, 3937.
(23) Frenkel, D.; Smit, B. *Understanding Molecular Simulation: From Algorithms to Applications*, 2nd ed.; Academic Press: San Diego, 2002.
(24) Sava, D. F.; Rodriguez, M. A.; Chapman, K. W.; Chupas, P. J.; Greathouse, J. A.; Crozier, P. S.; Nenoff, T. M. *J. Am. Chem. Soc.* **2011**, *133*, 12398.
(25) Sava, D. F.; Chapman, K. W.; Rodriguez, M. A.; Greathouse, J. A.; Crozier, P. S.; Zhao, H.; Chupas, P. J.; Nenoff, T. M. *Chem. Mater.* **2013**, *25*, 2591.
(26) Duren, T.; Bae, Y.-S.; Snurr, R. Q. *Chem. Soc. Rev.* **2009**, *38*, 1237.
(27) Varga, T.; Wilkinson, A. P.; Angel, R. J. *Rev. Sci. Instrum.* **2003**, *74*, 4564.
(28) Johari, G. P.; Jones, S. J. *Philos. Mag. B* **1986**, *54*, 311.
(29) Huang, Y.; Havenga, E. A. *Chem. Phys. Lett.* **2001**, *345*, 65.
(30) Wang, S.; Hirai, S.; Shapiro, M. C.; Riggs, S. C.; Geballe, T. H.; Mao, W. L.; Fisher, I. R. *Condens. Matter* **2012**, 1.
(31) Sun, Z.; Zhou, J.; Pan, Y.; Song, Z.; Mao, H.-K.; Ahuja, R. *Proc. Natl. Acad. Sci. U.S.A.* **2011**, *108*, 10410.
(32) Bennett, T. D.; Simoncic, P.; Moggach, S. A.; Gozzo, F.; Macchi, P.; Keen, D. A.; Tan, J.-C.; Cheetham, A. K. *Chem. Commun.* **2011**, *47*, 7983.
(33) Chapman, K. W.; Sava, D. F.; Halder, G. J.; Chupas, P. J.; Nenoff, T. M. *J. Am. Chem. Soc.* **2011**, *133*, 18583.
(34) Hu, Y. H.; Zhang, L. *Phys. Rev. B* **2010**, *81*, 174103/1.
(35) Cairns, A. B.; Catafesta, J.; Levelut, C.; Rouquette, J.; van der Lee, A.; Peters, L.; Thompson, A. L.; Dmitriev, V.; Haines, J.; Goodwin, A. L. *Nat. Mater.* **2013**, *12*, 212.
(36) Allan, D. R.; Clark, S. J.; Brugmans, M. J. P.; Ackland, G. J.; Vos, W. L. *Phys. Rev. B* **1998**, *58*, R11809.
(37) Serra-Crespo, P.; Stavitski, E.; Kapteijn, F.; Gascon, J. *RSC Adv.* **2012**, *2*, 5051.